

# Modelling the structure of clusters of $C_{60}$ molecules

Jonathan P. K. Doye<sup>†</sup> and David J. Wales

*University Chemical Laboratory, Lensfield Road, Cambridge CB2 1EW, United Kingdom*

Wolfgang Branz

*Max-Planck-Institut für Festkörperforschung, Heisenbergerstr. 1, 70569 Stuttgart, Germany*

Florent Calvo

*Laboratoire de Physique Quantique, IRSAMC, Université Paul Sabatier,  
118 Route de Narbonne, F31062 Toulouse Cedex.*

(Dated: October 28, 2018)

We locate putative global minima for  $(C_{60})_N$  clusters modelled by the potential of Pacheco and Prates-Ramalho up to  $N=105$ . These minima are based on icosahedral packing up to  $N=15$ , but above this size the lowest-energy structures are decahedral or close-packed. Although structures based on the 98-molecule Leary tetrahedron, which have been inferred from experiment, are not lowest in energy for this potential, an examination of the energetics of a growth sequence leading to the Leary tetrahedron lends further support to the experimental assignments. An analysis of the potential energy surface topography and the thermodynamics of two example clusters indicates that the multiple-funnel topography is likely to have a strong influence on the dynamics of structure formation and that solid-solid transitions driven by differences in vibrational entropy are likely to be common.

## I. INTRODUCTION

There has been much interest in the condensed-phase properties of  $C_{60}$  molecules because of their unusual intermolecular potential. At high temperature the molecules can rotate freely and so they act as large ‘pseudo-atoms’ with interactions that are extremely short-ranged relative to the large equilibrium pair separation. Consequently the properties of  $C_{60}$  can extend beyond the range of behaviour observed for atomic materials. For example, there are theoretical predictions that the liquid phase is unstable<sup>1,2</sup> or marginally stable<sup>3,4,5,6</sup> with the precise results depending on the potential (and somewhat on the methodology<sup>7</sup>) used.

There has also been considerable interest in the structural properties of clusters of  $C_{60}$  molecules, prompted by the first experiments of Martin *et al.* on positively-charged clusters.<sup>8</sup> This mass spectroscopic study revealed magic numbers for clusters with less than 150 molecules that are indicative of structures based upon Mackay icosahedra.<sup>9</sup> The stability of the icosahedral  $(C_{60})_{13}$  has since been further illustrated by Hansen *et al.*<sup>10,11</sup> However, subsequent calculations using the spherically-averaged Girifalco potential<sup>12</sup> found that icosahedral structures are only lowest in energy up to  $N=13$ .<sup>13,14,15</sup> Above this size the structures are either decahedral or close-packed. The rapid emergence of bulk-like structures for this potential contrasts with many other atomic

clusters where icosahedral structures can persist up to large sizes, for example, up to at least 20 000 atoms for sodium.<sup>16</sup> This behaviour, and the marginal stability of the liquid phase, has a common origin in the narrowness of the  $C_{60}$  intermolecular potential well. As the range of a potential is decreased, there is an increasing energetic penalty for strained structures, be they icosahedra<sup>17</sup> or liquid configurations,<sup>18,19</sup> which involve nearest-neighbour distances that deviate from the equilibrium pair distance.

One possible cause of the discrepancy between experiment and theoretical calculations is the isotropic nature of the Girifalco potential. However, calculations using an all-atom model also found that icosahedra are only lowest in energy at small sizes, albeit to slightly larger sizes ( $N=16$ ) than for the Girifalco potential.<sup>20,21,22</sup>

This situation led Shvartsburg and Jarrold to investigate the possibility of distinguishing icosahedral from decahedral and close-packed isomers by their mobility. However, the differences in the computed mobilities are small and were comparable to the experimental resolution.<sup>23</sup> More recently, Branz *et al.* performed some new mass spectroscopic experiments on  $(C_{60})_N$  clusters to try to obtain further insights into the difference between theory and experiment.<sup>24</sup> They found that the observed structures are independent of the sign and magnitude of the charge. However, temperature was found to be a key variable in determining the structure. The

initial cold as-grown clusters showed no magic numbers. Only on annealing at higher temperatures are the magic numbers revealed, as the relative evaporation rates cause larger populations to develop in those clusters that are more resistant to evaporation. After annealing at 490 K, as in the previous experiment, magic numbers consistent with icosahedral clusters are obtained. However, annealing at 585 K reveals a new set of magic numbers that correspond to non-icosahedral clusters.<sup>25</sup> As well as sizes associated with face-centred-cubic (fcc) and decahedral packing, particularly prominent were magic numbers associated with the recently discovered Leary tetrahedron.<sup>26</sup>

There are two possible explanations for this temperature dependence. Firstly, the results could reflect changes in the thermodynamically most stable structures with temperature. Such solid-solid transitions have now been observed in a variety of systems.<sup>17,27,28,29,30,31,32,33</sup> However, for all these examples icosahedral structures are more stable at higher temperature, and are favoured because they have a larger vibrational entropy.<sup>32</sup> Furthermore, the theoretical calculations for  $(C_{60})_N$  suggest that the non-icosahedral structures are lowest in energy and so would be favoured at low temperature. Indeed, such a transition to a high-temperature icosahedral structure has been located for  $(C_{60})_{14}$  interacting with the Girifalco potential<sup>33</sup> and has also been suggested for some larger clusters.<sup>34</sup> As the behaviour of these solid-solid transitions is opposite to that of the experiment, this explanation is unlikely.

Secondly, the icosahedral structures could be more accessible during the growth and annealing of the clusters, with escape from the icosahedral region of configuration space into the state with lowest free energy only being possible at the highest temperatures. This interpretation has support from a variety of sources. For example, it has been shown that it is possible, under certain conditions, to preferentially grow metastable icosahedral clusters for silver.<sup>35</sup> Furthermore, analyses of the potential energy surface (PES) topography of those Lennard-Jones clusters with non-icosahedral global minima has shown that large energy barriers exist for interconversion of the icosahedral isomers and the global minimum, and that the icosahedral funnel is much wider.<sup>36</sup> Thus, on relaxation down the PES, the system is likely to become trapped in the icosahedral region of configuration space. This trapping is partly due to the greater structural similarity to the polytetrahedral configurations typical of the liquid, but also to the general energetic preference that Lennard-Jones clusters have for icosahedral geometries.<sup>37</sup> The latter would not hold for clusters of  $C_{60}$  molecules. Finally, short-ranged potentials have been shown to lead to relatively large barriers<sup>38,39</sup> and consequently to much slower dynamics.<sup>40</sup> Therefore, it is plausible that kinetic effects could dominate for  $(C_{60})_N$  clusters on the experimental time scales, even for the relatively small clusters studied.

Many of the studies of the condensed-phase properties

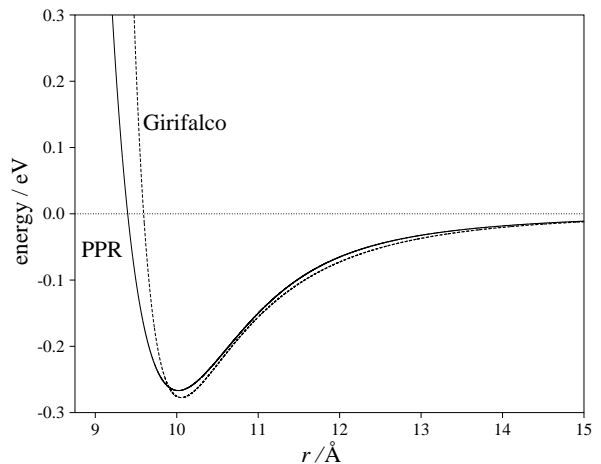


FIG. 1: Comparison of the PPR and Girifalco pair potentials.

of  $C_{60}$  have used the Girifalco potential.<sup>1,3,4,5,13,14,15,41</sup> However, a new single-site potential has recently been derived by Pacheco and Prates-Ramalho (PPR) that gives an improved description of many properties of bulk  $C_{60}$ , including, for example, the dependence of the density of the crystal on pressure.<sup>42</sup> Furthermore, the high-temperature thermodynamics of clusters interacting with this potential are in reasonable agreement with those of an all-atom potential.<sup>43</sup> Here, we see if this potential can help to explain the experimental observations of Branz *et al.*<sup>24</sup> Global optimization has been previously attempted for the PPR potential.<sup>34,44</sup> However, the conclusions of these papers are contradictory and, as we shall see, many of the putative global minima are sub-optimal. Here, as well as locating putative global minima for this potential, we also consider the most stable growth sequence for structures based on the experimentally observed Leary tetrahedra, and examine the PES topography and the thermodynamics of two example clusters.

## II. METHODS

The PPR potential consists of a pair potential plus a three-body term of the standard Axilrod-Teller form.<sup>45</sup> The potential energy of the cluster is therefore given by

$$E = \sum_{i<j} V_{\text{pair}}(r_{ij}) + C_{\text{AT}} \sum_{i<j<k} V_{\text{AT}}(r_{ij}, r_{ik}, r_{jk}), \quad (1)$$

where  $C_{\text{AT}}$  gives the magnitude of the Axilrod-Teller term. The pair potential consists of a Morse form for the short-range repulsion, a van der Waals expansion for the long-range attraction and a Fermi function to describe the crossover between these two regimes. The forms of these functions and the associated parameters are given in Ref. 42.

As one can see from Figure 1, the PPR pair potential has a softer repulsion than the Girifalco potential, leading to a wider potential well. This effect can be quantified by matching the second derivative at the bottom of the well to that of the Morse potential,

$$V_M(r) = \epsilon \exp[\rho(1 - r/r_{\text{eq}})] (\exp[\rho(1 - r/r_{\text{eq}})] - 2), \quad (2)$$

where  $\epsilon$  is the pair well depth and  $r_{\text{eq}}$  is the equilibrium pair distance. The Morse potential becomes increasingly narrow as the parameter  $\rho$  increases. The curvature at the bottom of the Morse well is  $2\rho^2$  when the units of energy and distance are the pair well depth and equilibrium pair distance. This result can then be used to obtain a value of  $\rho_{\text{eff}}$ , a measure of the effective range, for each potential. This analysis has been done previously for the Girifalco potential:  $\rho_{\text{eff}}^{\text{G}}=13.62$ .<sup>46</sup> For the PPR potential, however,  $\rho_{\text{eff}}^{\text{PPR}}=11.28$ . This difference in  $\rho_{\text{eff}}$  has a well-understood effect on the resulting properties of the liquid<sup>18,19,47</sup> and of clusters.<sup>17,48</sup> For example, it will make the bulk PPR liquid phase more stable, as has been observed.<sup>6</sup> More importantly for this study, it will make icosahedral structures more stable than for the Girifalco potential.

The three-body Axilrod-Teller term always gives rise to a positive contribution to the energy for a compact structure. For example, its inclusion leads to a 6% increase in the energy of the bulk  $\text{C}_{60}$  crystal.<sup>42</sup> However, in the global optimization study of Ref. 44, the supposed global minima for the full PPR potential had a lower potential energy than those when only the pair potential was used. This is clearly wrong and presumably must have been due to an error when coding the Axilrod-Teller term. Furthermore, in the other optimization study of PPR clusters, putative global minima were only located for the pair potential, because of the greater computational cost of the three-body term.<sup>34</sup>

The most unfavourable common configuration for the three-body Axilrod-Teller term is three nearest-neighbour molecules arranged in an equilateral triangle.<sup>49</sup> Therefore, one would expect the three-body energy to be larger for those structures that have more nearest neighbours, more polytetrahedral character and close-packed surfaces. Thus the Axilrod-Teller term disfavors icosahedral structures the most.<sup>50</sup>

To locate the global minima for the PPR potential we used basin-hopping<sup>51</sup> (Monte Carlo plus minimization<sup>52</sup>), which has proved to be a very effective method for a variety of cluster systems. This approach<sup>51,53</sup> and the reasons for its success<sup>27,54,55</sup> have been described in detail elsewhere. The only specific modification for the present application was to reduce the computational cost of the minimizations by only switching on the three-body interactions close to convergence. Such a ‘guiding function’ approach has previously been suggested and exploited by Hartke.<sup>56</sup> As well as basin-hopping, we also reoptimized a large database of minima that we had obtained from previous optimization studies

on Lennard-Jones,<sup>51</sup> Morse<sup>17,48</sup> and Girifalco<sup>15</sup> clusters. Most of the global minima that we located were contained within this database.

To generate the samples of minima from which the disconnectivity graphs and the thermodynamics in Section IV were calculated, we used the same methods as those we have previously applied to LJ<sup>30,36,57</sup> and Morse<sup>39</sup> clusters. We thereby obtain large samples of connected minima and transition states that provide good representations of the low-energy regions of the PES. The approach involves repeated applications of eigenvector-following<sup>58</sup> to find new transition states and the minima they connect, as described in detail elsewhere.<sup>59</sup>

### III. GLOBAL MINIMA

Putative global minima were located for the full PPR potential up to  $N=105$ , the size range of interest for comparison with the high temperature experiments of Branz *et al.*<sup>24</sup> The energies and point groups of these structures are given in Table I and coordinates are available on the world-wide web from the Cambridge Cluster Database.<sup>60</sup>

As expected, the energies of the global minima differ from those reported in Ref. 44, because of the error in the Axilrod-Teller term. To facilitate comparisons with the other results in Refs. 34 and 44, we also report the energies of these global minima when reoptimized for the PPR pair potential (Table I). The resulting energies will not necessarily be the global optima for the pair potential, but they should provide a good upper bound. Comparisons with these energies show that the putative global minima for the PPR pair potential given in Ref. 44 are sub-optimal for  $N \geq 19$  and those in Ref. 34 are sub-optimal for  $N=18, 26, 33-36$  and  $N \geq 40$ . Only for  $N=16$  and 29 are lower two-body energies obtained in these papers,<sup>34,44</sup> indicating that for these cluster sizes the introduction of the Axilrod-Teller term leads to a change in the structure of the global minimum. For  $N=16$  the relevant minimum is icosahedral with  $E=-13.006550$  eV and  $E_2=-13.447202$  eV, and for  $N=29$  it is an alternative decahedral minimum with  $E=-27.540094$  eV and  $E_2=-28.516282$  eV.

In Figure 2a we plot the energies of the PPR global minima so that particularly stable clusters stand out. We also provide a comparison with results for the Girifalco potential (Figure 2b), partly because a significant number of the putative global minima in Ref. 15 have now been improved (an up-to-date list is maintained at the Cambridge Cluster Database<sup>60</sup>). A selection of the global minima are depicted in Figure 3.

At  $N=13$  the icosahedral global minimum is noticeably more stable than for the Girifalco potential, which is consistent with the PPR potential’s slightly wider well. Furthermore, icosahedral structures are lowest in energy up to 15 molecules, or up to 16 molecules if the Axilrod-Teller term in the potential is not included—as noted in

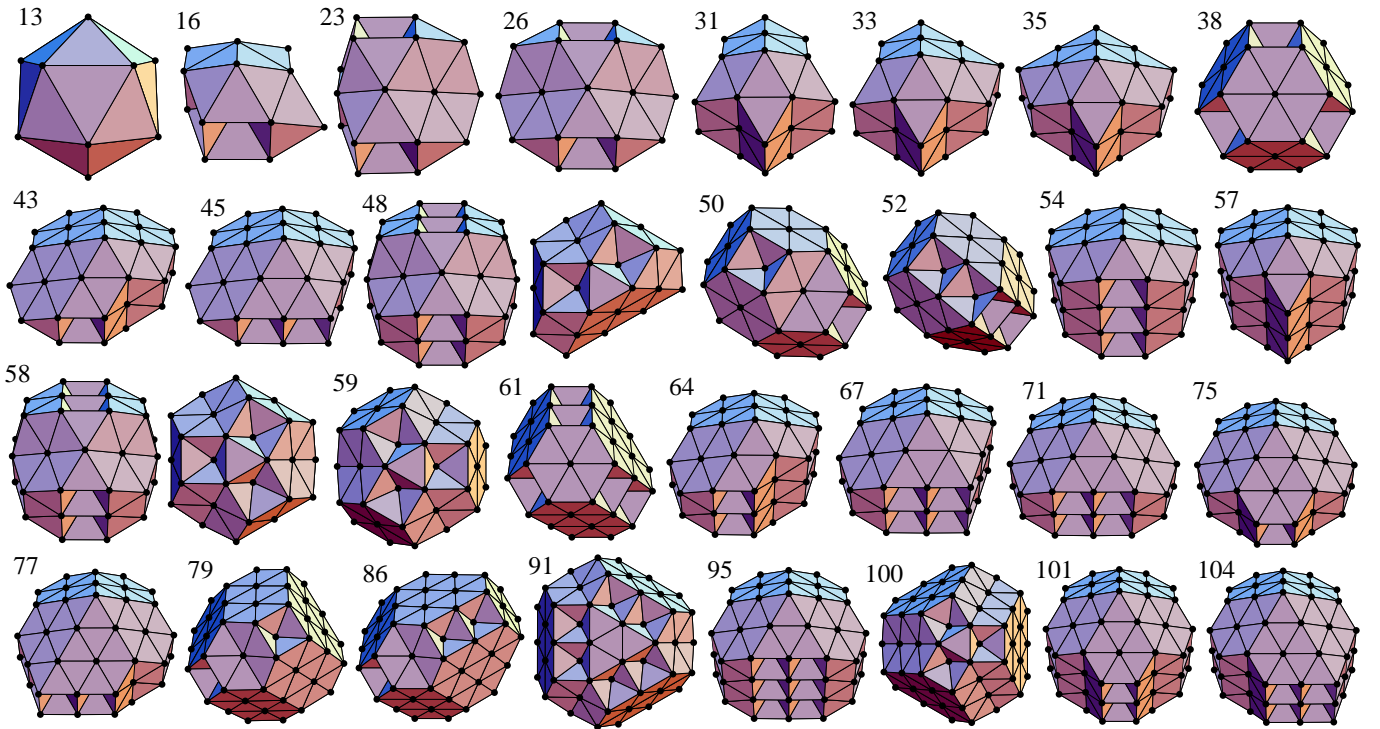


FIG. 3: A selection of the global minima for the PPR potential. Each molecule is represented by a point at the molecular centre. The two views of the 48- and 58-molecule clusters illustrate the relationship of these structures to both decahedra and the Leary tetrahedron.

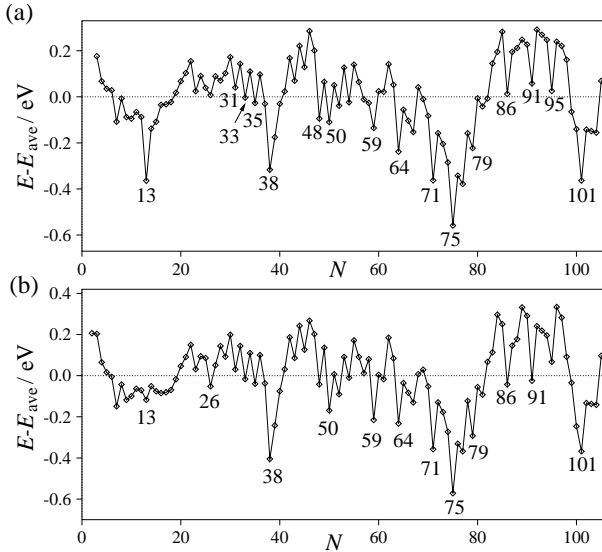


FIG. 2: Energies of the global minima for  $(C_{60})_N$  clusters modelled by the (a) PPR and (b) Girifalco potentials. The energy zero is taken to be  $E_{ave}$ , a four-parameter fit to the energies of the global minima. For the PPR potential  $E_{ave}/eV = -1.6537N + 2.1901N^{2/3} + 0.1263N^{1/3} - 0.7467$ . For the Girifalco potential  $E_{ave}/eV = -1.789N + 2.294N^{2/3} + 0.5907N^{1/3} - 1.292$ .

Section II this term slightly disfavours icosahedral structures. However, contrary to the claims of Refs. 34 and 44 there are no further icosahedral global minimum above this size. Instead decahedral or close-packed clusters are lowest in energy.

To illustrate how the relative stabilities of icosahedral structures with respect to the global minimum evolve with size, we give the energy differences for examples where particularly stable fcc and icosahedral forms are available. At  $N=38$  the difference in energy between the fcc truncated octahedron and the lowest-energy icosahedral structure is 0.582 eV. However, at  $N=55$  the Mackay icosahedron is 0.297 eV above the decahedral global minimum. When the Axilrod-Teller interactions are not included this difference decreases to 0.159 eV, again illustrating that this term slightly disfavours icosahedra. In contrast, the energy difference for the Girifalco potential is a considerably larger 1.997 eV. These results are consistent with the behaviour expected from the respective values of  $\rho_{eff}$ : the Mackay icosahedron is lowest in energy for the Morse potential up to  $\rho=11.15$  and then becomes increasingly unstable as the width of the potential decreases further.

The pronounced minima in Figure 2 correspond to particularly low-energy structures that could potentially give rise to magic numbers. Comparing (a) and (b) of Figure 2 it is apparent that the patterns are very similar, indicat-

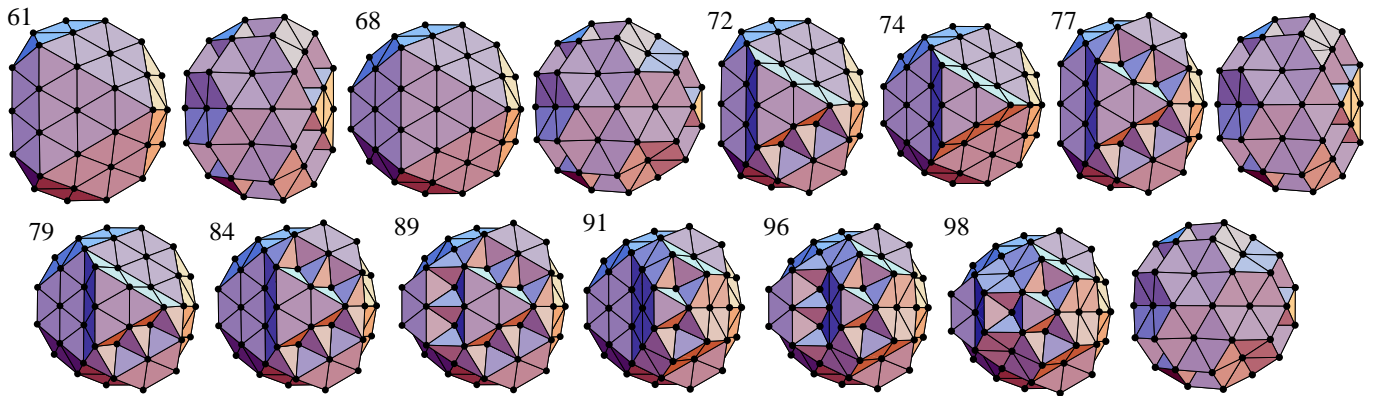


FIG. 4: Particularly stable clusters on the growth sequence leading to the Leary tetrahedron. When two viewpoints are given they correspond to the front and back of the cluster.

ing that the two  $C_{60}$  potentials favour similar structures. Prominent in both figures are the same particularly stable decahedral and close-packed forms, most of which are illustrated in Figure 3. The main differences are that, for the Girifalco potential, the feature due to  $(C_{60})_{13}$  is much less pronounced, for the reasons explained above, and that the close-packed structures are somewhat more favoured. The latter feature is again due to the shorter range of the Girifalco potential, as is the greater number of close-packed global minima for the Girifalco potential.

There is some correspondence between Figure 2 and the high temperature magic numbers observed experimentally.<sup>24</sup> Small peaks in the mass spectrum at  $N=31$ , 33 and 35 probably correspond to a series of small decahedra. Similarly, the peak at  $N=38$  can be assigned to the fcc truncated octahedron, and the peaks at  $N=64$ , 71 and 75 are probably due to Marks decahedra. Particularly interesting is the feature in Figure 2 corresponding to the decahedral  $(C_{60})_{48}$  global minimum, because the most prominent peak in the mass spectrum occurs at  $N=48$ . Like a number of the other decahedral global minima, this structure has an overlayer on the  $\{111\}$  faces in sites which are hcp with respect to the five slightly strained fcc tetrahedra that are the basis of decahedral structures. In fact, many of these structures are fragments of larger Mackay icosahedra with the apex of the decahedron corresponding to what would become the centre of the icosahedron. Indeed, growth simulations for silver have indicated that the addition of this overlayer does provide a natural pathway to the growth of larger icosahedra.<sup>35</sup>

However, many of the particularly stable structures, especially for  $N \geq 50$ , do not correspond to magic numbers in the experiment. There are no experimental peaks corresponding to the close-packed tetrahedra at  $N=59$  and 100, nor to the twinned truncated octahedra at  $N=50$  and 79 and the 101-molecule Marks decahedron. Instead, peaks occur in the mass spectrum at  $N=58$ , 61, 68, 77, 84, 91, 96 and 98, which cannot be simply explained by

reference to the global minima of model  $C_{60}$  potentials. These peaks have previously been assigned<sup>24</sup> to structures based on a 98-molecule Leary tetrahedron.<sup>26</sup> This recently discovered structure is illustrated in Figure 4. It can be described in terms of five fcc tetrahedra arranged into a stellated tetrahedron with apex molecules removed and 7-molecule hexagonal patches covering the edges of the central tetrahedron. That this structure is not the global minimum for the PPR or Girifalco potential is consistent with the values of  $\rho_{\text{eff}}$ . For the Morse potential it is only the global minimum for  $6.91 < \rho < 9.45$  because it has a strain energy intermediate between decahedra and icosahedra.

To attempt to add further weight to the experimental assignments we calculated the energies of a series of structures derived from the Leary tetrahedron. Although they are not lowest in energy, the size variation of their energies, plotted for  $60 < N < 100$  in Figure 5, is insightful. There is remarkable agreement between the features in this graph and the remaining magic numbers.

The stable structures for the Leary tetrahedral growth sequence are illustrated in Figure 4. The 91-molecule structure is derived by removing a hexagonal patch from over one of the edges of the central tetrahedron. In contrast, to obtain the 89-molecule structure one of the points of the Leary tetrahedron is further truncated. By a similar truncation the  $(C_{60})_{91}$  global minimum can be derived from the 100-molecule tetrahedral global minimum (Figure 3). Most of the other structures can be obtained by a combination of these two changes. The 84-molecule structure is derived by a truncation and the removal of an adjacent patch. Similarly, truncation of two of the fcc tetrahedra and the removal of the common patch gives the 77-molecule structure. The 68-molecule structure is derived by completely removing one of the fcc tetrahedra and adjacent patches, thus giving a structure that is also a fragment of the 147-molecule Mackay icosahedron. The truncation of a further tetrahedron leads to the 61-molecule structure.

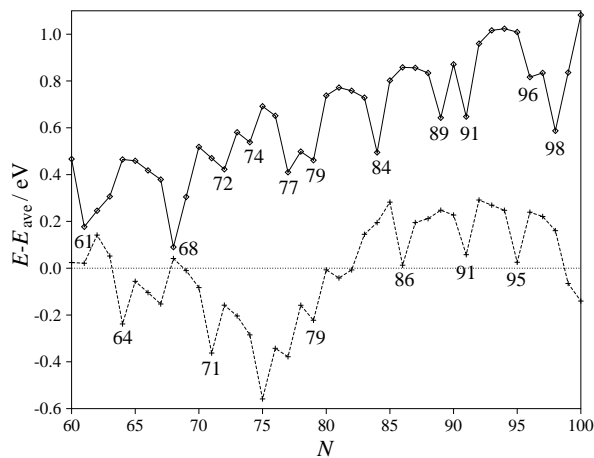


FIG. 5: Energies of structures based upon the 98-molecule Leary tetrahedron (solid line) compared to the energies of the global minima (dashed line) for the PPR potential.

Interestingly, the latter two structures are global minima for Morse clusters, but were not located in the most recent optimization study.<sup>48</sup> They have energies of  $E_{61}(\rho=10)=-252.488332\epsilon$  and  $E_{68}(\rho=10)=-286.643320\epsilon$ , and are lowest in energy in the ranges  $9.42 < \rho < 10.34$  and  $7.40 < \rho < 11.55$ , respectively.

The prominence of the peak in the mass spectrum at  $N=48$  also fits with this preference for structures based upon the Leary tetrahedron. The second view of the decahedral  $(C_{60})_{48}$  global minimum in Figure 3 shows that it is also a fragment of the Leary tetrahedron. By adding an identical overlayer to the bottom  $\{111\}$  faces of this cluster the decahedral  $(C_{60})_{58}$  global minimum is obtained, which is again a fragment of the Leary tetrahedron. Although this cluster is not especially stable compared to nearby sizes for the PPR potential, its relationship to the Leary tetrahedron provides a basis for confidently assigning the remaining magic number at  $N=58$  to this structure.

#### IV. $(C_{60})_{38}$ AND $(C_{60})_{55}$

Although the location of the global minima should be the first step in the theoretical determination of a cluster's structure, the thermodynamics<sup>32</sup> and dynamics<sup>61</sup> can also play an important role. Here, we examine the behaviour of two example clusters in more detail. We choose  $(C_{60})_{38}$  and  $(C_{60})_{55}$  because particularly stable fcc (38) and icosahedral (55) structures are possible. Furthermore, these sizes have been extensively studied for the longer-ranged Lennard-Jones potential.<sup>27,30,36,40,62,63</sup>

In order to construct disconnectivity graphs for these two clusters we have generated large samples of min-

ima and transition states, plus the pathways connecting them. As this is a computationally demanding task only the two-body component of the PPR potential was used. The graphs for the full potential would be very similar; the main effect of the introduction of the three-body term would be to displace the icosahedral regions of configuration space further up in energy. We located 38 558 minima and 39 959 transition states for  $N=38$  and 39 043 minima and 39 845 transition states for  $N=55$ .

Disconnectivity graphs<sup>64,65</sup> provide a representation of the barriers between minima on a PES.<sup>64,65</sup> In a disconnectivity graph, each line ends at the energy of a minimum. At a series of equally-spaced energy levels we determine which (sets of) minima are connected by paths that never exceed that energy. We then join up the lines in the disconnectivity graph at the energy level where the corresponding (sets of) minima first become connected. In a disconnectivity graph an ideal single-funnel<sup>66,67</sup> PES would be represented by a single dominant stem associated with the global minimum to which the other minima directly join. For a multiple-funnel PES there would be a number of major stems that only join at high energy. A single funnel PES is typically associated with efficient relaxation to the global minimum, whereas for a multiple-funnel PES there is a separation of time scales between relaxation to a low-energy structure and inter-funnel equilibrium.<sup>59</sup>

For  $(C_{60})_{38}$  and  $(C_{60})_{55}$  it is not possible to characterize the whole PES because of the huge numbers of minima. Besides, even if we could perform such a characterization, any attempt at representation using a disconnectivity graph would just be obscured by the density of lines. Therefore, we concentrate on the low-energy regions of the PES that are of most importance when considering structure, and only include the lines leading to the lowest 250 minima.

For both clusters the PES topography has a multiple-funnel character, where each funnel corresponds to a different structural type (Figure 6). For this short-ranged potential, there are a number of competing low-energy morphologies that are separated by large energetic barriers. As the barriers between minima of the same structural type are typically much smaller, the graphs clearly separate the different morphologies.

This behaviour contrasts with that for Lennard-Jones clusters, which (with some notable exceptions) typically have a single-funnel topography that is dominated by icosahedral structures.<sup>36</sup> However, for the PPR potential the difference in energy between close-packed and decahedral structures is small. Furthermore, there are often a number of close-packed forms possible that have significant structural differences. For example, for  $(C_{60})_{55}$  the close-packed region of configuration space divides up into structures that are based on the 50-molecule global minimum (the twinned truncated octahedron) and those based on the 59-molecule tetrahedral global minimum (Figure 3). Additionally, as well as a funnel leading to the conventional decahedral global minimum, there is a

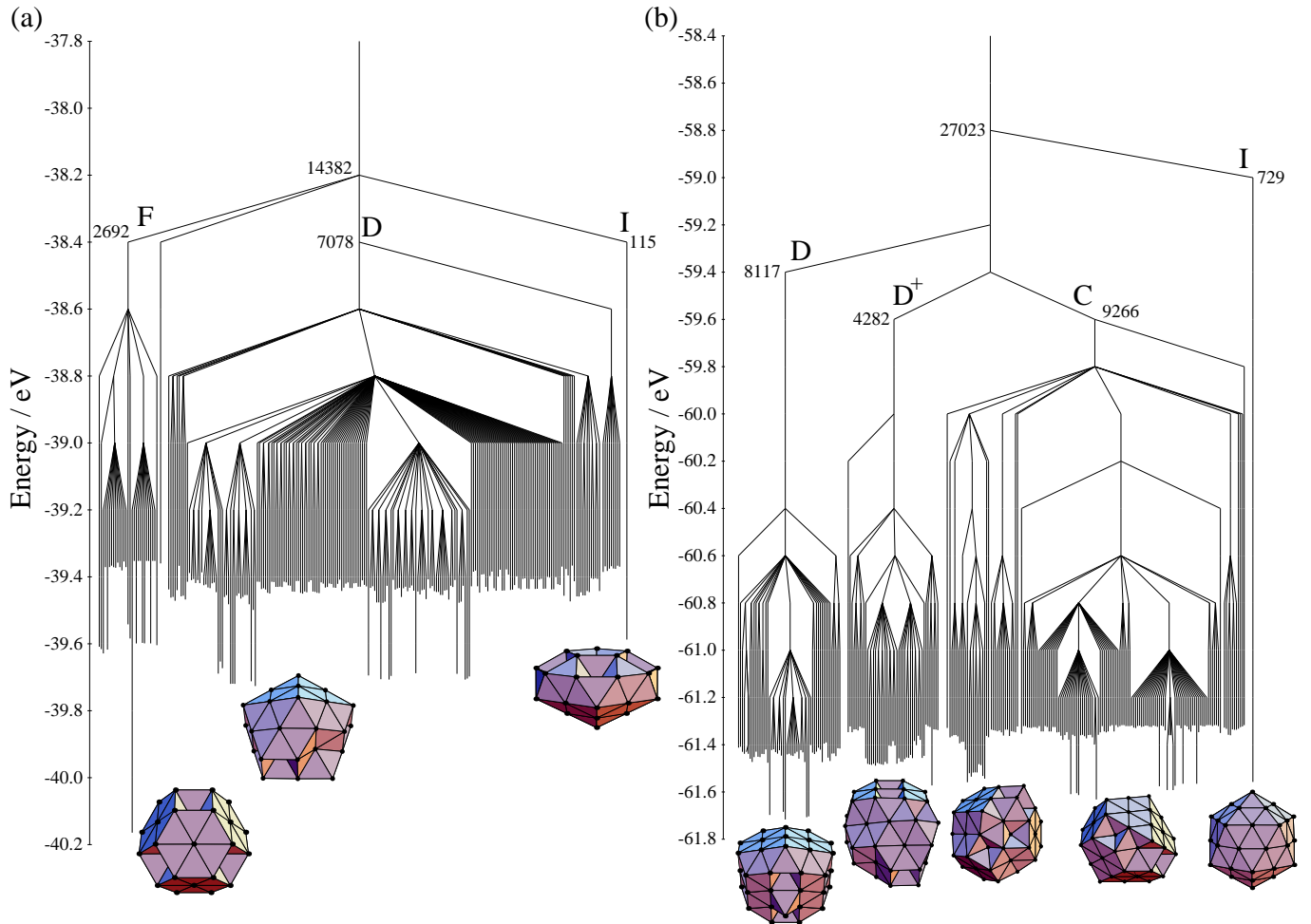


FIG. 6: Disconnectivity graphs for (a)  $(C_{60})_{38}$  and (b)  $(C_{60})_{55}$ . Lines corresponding to the lowest 250 minima are represented. Structural labels have been placed adjacent to the lines corresponding to the different funnels on the PES, where, as in Table I, I stands for icosahedral, D for decahedral ( $D^+$  have an overlayer on the  $\{111\}$  faces), F for fcc and C for close-packed. The numbers refer to the number of minima below the corresponding node in the full graph. Pictures of the lowest-energy minima for the different structural types have been placed adjacent to the corresponding lines.

low-energy region of configuration space corresponding to decahedral structures that have the  $\{111\}$  faces partially covered. These latter structures can be constructed by adding molecules to the 48-molecule global minimum. This complexity of the  $(C_{60})_{55}$  disconnectivity graph contrasts with that of  $(C_{60})_{38}$ , for which there are only funnels associated with the three basic morphologies.

The disconnectivity graphs can tell us a lot about the dynamics of these two clusters. On the disconnectivity graphs we give the numbers of minima in our sample that are associated with each funnel. Although, these are large underestimates of the true values because of the incompleteness of our samples, they do provide a reasonable indication of the relative numbers of low-energy minima of each structural type, and hence of the widths of the funnels in configurational terms. It is particularly

noticeable that there are far fewer low-energy icosahedral minima, as expected for a short-ranged potential. By contrast, the number of decahedral and close-packed structures is of the same order.

Based on this information, on relaxation down the PES one would expect the system to be more likely to end up in a close-packed or decahedral configuration. However, there are other factors that can influence the dynamical behaviour. There is a vibrational, as well as a configurational, contribution to the width of a funnel. This term is larger for the icosahedral funnel because the associated minima are generally flatter and wider. Furthermore, it may also be that the icosahedral structures lie, in some sense, closer to the liquid-like region of configuration space because of their greater polytetrahedral character.<sup>19,68</sup>

Structure formation in clusters does not necessarily occur by relaxation from a high-energy state, but can also occur by growth from a smaller pre-existing solid cluster.<sup>61</sup> Although the width of the funnels is less important in this case, the disconnectivity graphs can still be useful because they give an idea of the kinetic stability of the possible structures. The large barriers between funnels suggest that, except at high temperature, trapping will occur within the funnel of the existing structure, even if the structure is metastable. Indeed escape from a funnel will become more difficult with increasing size because the interfunnel barriers become larger.

Therefore, during cluster growth, except at high temperatures and extremely long time scales, the smaller clusters serves as templates for growth and only the optimization of the position of additional loosely-bound molecules is likely to occur. If icosahedral structures are preferred at the last size for which equilibrium is possible, then larger icosahedra will result. Thus, the disconnectivity graphs give additional support to the idea that icosahedra are observed experimentally because of kinetic trapping at low temperature.

To examine the low-temperature thermodynamics of the two clusters in question we use the harmonic superposition method.<sup>59,69</sup> In this approach the partition function is constructed by summing the partition functions of the individual minima on the PES. In the harmonic approximation, we obtain

$$Z = \sum_i \frac{n_i \exp(-\beta E_i/kT)}{(\beta \hbar \bar{\nu}_i)^{3N-6}}, \quad (3)$$

where  $E_i$  is the energy of minimum  $i$ ,  $\bar{\nu}_i$  is the geometric mean frequency and  $n_i$  is the number of permutational isomers ( $2N!/h_i$ , where  $h_i$  is the order of the point group).

This approach is unable to reproduce high temperature behaviour such as melting in the present cases, because no effort has been made to compensate for the incompleteness of our samples of minima, thus leading to an underestimate of the configurational entropy of the high-energy states. It is possible to overcome this limitation by using information obtained from an ergodic simulation,<sup>59,69</sup> but this is not attempted because ergodicity is hard to achieve for these clusters and because we are more interested in solid-solid transitions, for which we only need to characterize the low-energy regions of the PES. Instead we used parallel-tempering to locate the point at which the cluster melts or boils. It is also possible to introduce anharmonicity into this scheme,<sup>70,71</sup> however this additional level of complexity is unnecessary for the insights we are seeking to achieve here.

The advantage of the superposition method is the ease with which the low-temperature thermodynamics can be obtained even when, as with  $(C_{60})_N$  clusters, there are large interfunnel energy barriers present. In fact it is not clear if any other method would be able to probe this regime, because of the difficulty of achieving ergodicity.

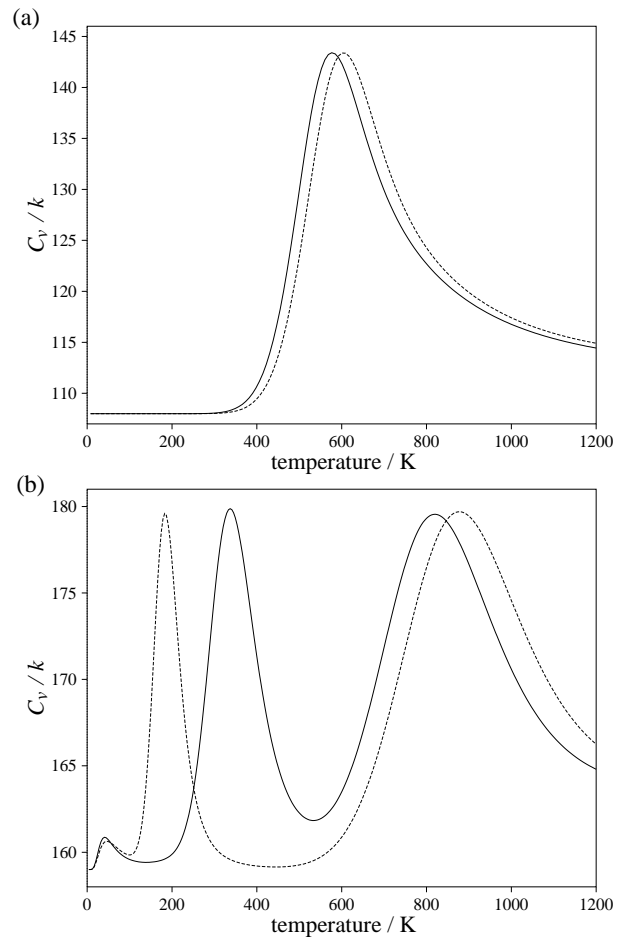


FIG. 7: Heat capacity curves for (a)  $(C_{60})_{38}$  and  $(C_{60})_{55}$  obtained from our samples of minima using the harmonic superposition method. The solid lines are for the full potential and the dashed lines are for the two-body potential.

Even techniques based on parallel tempering,<sup>72,73</sup> which are the only direct simulation methods that have been shown to succeed for challenging cases involving low-temperature solid-solid transitions in clusters,<sup>31,74</sup> failed for  $(C_{60})_{55}$ . The success of these methods relies on the coupling of the low-temperature runs to ergodic high-temperature runs involving molten clusters. However, because of the narrowness of any range of stability for the liquid-like state of clusters of  $C_{60}$  molecules<sup>41,43</sup> this is very hard to achieve.

Heat capacity curves for the two clusters are presented in Figure 7. These were calculated using the same samples of minima as for the disconnectivity graphs. It was also possible to reoptimize all the minima for the full potential. Both clusters show some evidence of solid-solid transitions.

For  $(C_{60})_{55}$  the energy gap between the icosahedral minima and the global minimum is relatively small and so a transition to the Mackay icosahedron occurs sig-



nificantly below the melting temperature. For the full potential this transition occurs at 377 K and, consistent with the reduction in the energy gap, at 184 K when the three-body term is neglected. Interestingly, there is also a small peak at  $\sim 45$  K, which corresponds to a redistribution of the equilibrium occupation probability amongst the five lowest-energy decahedral isomers. These minima are almost isoenergetic and correspond to the five different positions that the four-coordinate surface molecules can occupy. The high-temperature peak corresponds to the beginnings of the melting/boiling transition, which as expected is underestimated by the harmonic superposition method. Parallel tempering indicates that the actual peak for this transition is much larger and occurs at  $\sim 950$  K, although the result is somewhat dependent on the size of the constraining box in which the cluster is placed.

For  $(C_{60})_{38}$  the calculated heat capacity curve is much simpler and only has a single peak. This corresponds to the transition out of the truncated octahedron, first roughly equally into the low-energy decahedral minima and lowest-energy icosahedral minimum, and then at slightly higher temperature into the higher-energy states. As these transitions are so close together in temperature there is only a single peak in the heat capacity, which is centred on the initial transition because of the underestimation of the latent heat of melting by the present approach. Parallel tempering simulations suggest that the preliminary solid-solid transition gives rise to a shoulder in the melting peak, which occurs at  $\sim 900$  K.

Although we have only considered two sizes in detail, the large temperature window for which the Mackay icosahedron is most stable indicates that solid-solid transitions are likely to be common for other sizes. The results confirm what has been emphasized elsewhere, namely that crossover sizes at which the dominant structure changes depend on temperature.<sup>32</sup> So, although none of the clusters above  $N=15$  have icosahedral global minima, icosahedra can still be thermodynamically most stable for some range of temperature above this size. For example, similar calculations indicate that for  $(C_{60})_{19}$  icosahedral structures are favoured above 333 K. However, these results cannot explain the experimental observation of icosahedra, because they are seen at low not high temperature.

As for the solid-solid transitions that have been investigated in detail for Lennard-Jones clusters,<sup>32,75</sup> the above transitions are driven by the larger vibrational entropy of the icosahedral structures. For  $N=38$   $\bar{\nu}_{\text{icos}}:\bar{\nu}_{\text{deca}}:\bar{\nu}_{\text{cp}}=0.920:0.977:1$  and for  $N=55$   $0.909:1:0.999$ , where we have used the values for the lowest-energy minimum of each structural type. These differences are much larger than for Lennard-Jones clusters, where, for example,  $\bar{\nu}_{\text{icos}}:\bar{\nu}_{\text{deca}}:\bar{\nu}_{\text{cp}}=1:1.000:0.990$  for LJ<sub>55</sub> and the systematic differences between compact sequences of structures are no larger than 2% (Mackay icosahedra having the lowest frequencies).<sup>75</sup>

$\bar{\nu}$  is a measure of how the energy increases as the struc-

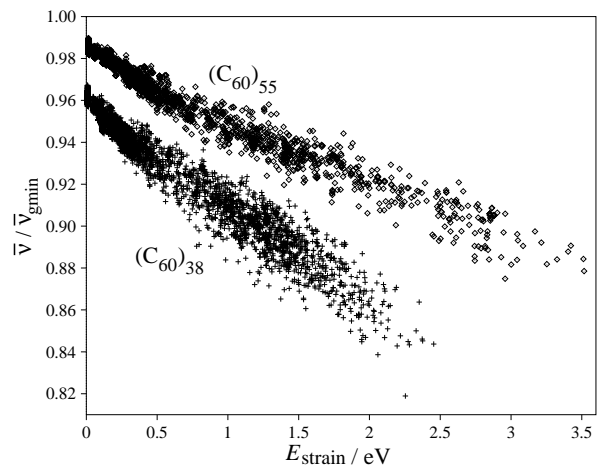


FIG. 8: The dependence of  $\bar{\nu}$  on  $E_{\text{strain}}$  for  $(C_{60})_{38}$  minima with  $n_{\text{nn}}=139$  (crosses) and  $(C_{60})_{55}$  minima with  $n_{\text{nn}}=217$  (diamonds). These samples contain 8408 and 7337 minima, respectively, and correspond to the largest subsets of the complete samples that have the same value of  $n_{\text{nn}}$ . The mean frequency is measured with respect to that for the global minimum.

ture is distorted, and so we can gain insight into the origins of the dependence of  $\bar{\nu}$  on structure if we examine the different contributions to the energy. For a pair potential

$$E = -n_{\text{nn}}\epsilon + E_{\text{strain}} + E_{\text{nnn}}, \quad (4)$$

where  $n_{\text{nn}}$  is the number of nearest neighbours (defined using a distance criterion  $r_0$ ), the strain energy, the energetic penalty for distances deviating from the equilibrium pair distance, is given by

$$E_{\text{strain}} = \sum_{i < j, r_{ij} < r_0} V(r_{ij}) + \epsilon \quad (5)$$

and the energy of non-nearest neighbours by

$$E_{\text{nnn}} = \sum_{i < j, r_{ij} > r_0} V(r_{ij}). \quad (6)$$

As  $E_{\text{nnn}}$  is small for a short-ranged potential and does not vary strongly with distance the main contributions to  $\bar{\nu}$  come from nearest neighbours. Therefore, it is clear that the more nearest neighbours a structure has the greater the effect on the energy. Thus, compact structures with few low-coordinate surface molecules have larger vibrational frequencies. This is the reason that  $\bar{\nu}$  generally decreases as the energy of the minima increases.

The strain energy also has a significant effect on the vibrational frequencies. For an unstrained structure all nearest neighbours lie at the equilibrium separation, and so any distortion of the structure leads to an increase in all the individual nearest-neighbour pair energies. For a strained structure, there is a dispersion of nearest-neighbour distances and so a distortion is likely to cause

some of them to deviate further from the equilibrium distance, but others to become closer. This compensation leads to a smaller rise in the energy, and hence to smaller vibrational frequencies. When the effect is isolated by only comparing minima with the same number of nearest neighbours, this trend is clear (Figure 8).

As the curvature of the pair potential increases, the effect of strain becomes larger. We can therefore explain both the much lower frequencies for the icosahedral structures in our two examples and why this effect is more dramatic than for Lennard-Jones clusters. Therefore, as the range of the potential is decreased, the increasing energy gap between icosahedra and the lowest-energy structures is compensated by a lower relative mean vibrational frequency and so it is still possible that icosahedral structures are stable for some range of temperature, even when the potential is relatively short-ranged.

The differences in  $\bar{\nu}$  between close-packed and decahedral structures are smaller, because of the smaller differences in the strain energy. Indeed, for  $(C_{60})_{55}$  the lowest-energy decahedral minima actually has a higher  $\bar{\nu}$  because the effect of a larger  $E_{\text{strain}}$  is more than compensated by the effect of a greater  $n_{\text{nn}}$ .

As Leary tetrahedra have a strain energy intermediate between icosahedra and decahedra, one would expect that their mean vibrational frequency is lower than for decahedral and close-packed clusters. Indeed, this is the case. For example, for  $(C_{60})_{98}$   $\bar{\nu}_{\text{icos}}:\bar{\nu}_{\text{Leary}}:\bar{\nu}_{\text{deca}}:\bar{\nu}_{\text{cp}}=0.925:0.972:0.997:1$ . Although the Leary tetrahedron does develop a small equilibrium population near to the melting point in the current model, there is no clear transition at which the Leary tetrahedron becomes the dominant structure.

## V. CONCLUSIONS

Putative global minima for the  $C_{60}$  intermolecular potential of Pacheco and Prates-Ramalho have been located for all clusters containing up to 105 molecules. For  $N \leq 15$  the structures follow an icosahedral growth sequence, but above this size the global minima are either decahedral or close-packed, with close-packed clusters becoming more common as the size increases. This progression to structures with lower strain energy as the size increases is expected, but is more rapid than for most atomic clusters, because the PPR potential is much more short-ranged than typical interatomic potentials.

The correspondence between many of the particularly low-energy PPR clusters and the high temperature experimental magic numbers adds further support to the interpretation that these sizes have particularly low free energies because they are particularly low in potential energy. This interpretation also implies that the icosahedral magic numbers seen at lower temperature are kinetic in origin. The large interfunnel barriers evident from the disconnectivity graphs of  $(C_{60})_{38}$  and  $(C_{60})_{55}$  add further

support to this hypothesis by indicating the difficulty of major structural transformations in a growing cluster. Moreover, preliminary results from growth simulations confirm this scenario.<sup>76</sup>

However, there are still discrepancies between the high temperature magic numbers and the low-energy model  $C_{60}$  clusters. Firstly, the magic number at  $N=19$ , which persists up to high temperature, is probably due to the double icosahedron. This perhaps suggests that the PPR potential is still effectively too short-ranged, but an alternative explanation is the thermal stabilization of this structure at the experimental temperature.

Secondly, a particular preference for structures that are based on the Leary tetrahedron is not reproduced. It is possible that these structures are only lowest in free energy at high temperature, but this seems unlikely for two reasons. Firstly, as the entropy is not so strongly size-dependent as the energy, magic numbers associated with structures that are entropically preferred are likely to be less pronounced. However, in the present case the magic numbers associated with the structures based upon the Leary tetrahedron are the most prominent. Secondly, no such transition is seen for  $(C_{60})_{98}$ . Hence, it is more likely that the discrepancy is due to the potential, and again suggests that the PPR potential is effectively too short-ranged. For the Morse potential the 98-atom Leary tetrahedron is lowest in energy for  $6.91 < \rho < 9.45$ . However, the situation is somewhat more complex. Only at a few sizes are structures based on the Leary tetrahedron actually the global minimum of the Morse potential. Therefore, the observed preference cannot simply be explained by the effective range. It is most likely to be related to the orientational degrees of freedom that are neglected in a single-site potential, such as the PPR model.

The thermodynamics calculations also indicate further discrepancies between experiment and the PPR model. We saw in Section IV that icosahedral structures are thermodynamically favoured at high temperature for certain sizes, because of their larger vibrational entropy. However, except perhaps for  $N=19$ , there is no experimental support for this scenario.

Although all-atom potentials have been employed for modelling clusters of  $(C_{60})$  molecules,<sup>20,21,22</sup> the double icosahedron was found not to be lowest in energy for  $N=19$  and the potentials were not applied in the size range relevant to structures based on the Leary tetrahedron. Furthermore, these types of all-atom potential are unable to reproduce the low-temperature properties of bulk  $C_{60}$ —the molecules have the incorrect orientation in the low-temperature crystal.<sup>77</sup> Although, at the temperatures relevant to experiment, the molecules are expected to be able to rotate freely,<sup>78</sup> it could well be that the energetic preferences for structures in which the molecules can have the preferred orientations will persist up to higher temperature. Therefore, to reproduce the preference for Leary tetrahedra it is likely that a potential that can give the correct orientations in the crystal is

required. There are a number of such potentials,<sup>79,80,81</sup> however this orientational preference has sometimes been achieved through the introduction of unrealistic electrostatic properties for the C<sub>60</sub> molecule.<sup>82</sup> Still, it would be interesting to know if these potentials do favour Leary tetrahedra. However, this would be an extremely challenging task computationally, both because of the complexities of the potentials and the huge number of possible orientational isomers for such large clusters.

### ACKNOWLEDGMENTS

JPKD is grateful to Emmanuel College, Cambridge for financial support.

### REFERENCES

- <sup>†</sup> Electronic address: jon@clust.ch.cam.ac.uk
- <sup>1</sup> M. H. J. Hagen *et al.*, *Nature* **365**, 425 (1993).
  - <sup>2</sup> J. Q. Broughton, J. V. Lill, and J. K. Johnson, *Phys. Rev. B* **55**, 2808 (1997).
  - <sup>3</sup> A. Cheng, M. L. Klein, and C. Caccamo, *Phys. Rev. Lett.* **71**, 1200 (1993).
  - <sup>4</sup> C. Caccamo, D. Costa, and A. Fucile, *J. Chem. Phys.* **106**, 255 (1997).
  - <sup>5</sup> M. Hasegawa and K. Ohno, *J. Chem. Phys.* **111**, 5955 (1999).
  - <sup>6</sup> A. L. C. Ferreira, J. M. Pacheco, and J. P. Prates-Ramalho, *J. Chem. Phys.* **113**, 738 (2000).
  - <sup>7</sup> M. Hasegawa and K. Ohno, *J. Chem. Phys.* **113**, 4315 (2000).
  - <sup>8</sup> T. P. Martin, U. Näher, H. Schaber, and U. Zimmermann, *Phys. Rev. Lett.* **70**, 3079 (1993).
  - <sup>9</sup> A. L. Mackay, *Acta Cryst.* **15**, 916 (1962).
  - <sup>10</sup> K. Hansen, H. Hohmann, R. Müller, and E. E. B. Campbell, *J. Chem. Phys.* **105**, 6088 (1996).
  - <sup>11</sup> K. Hansen, H. Hohmann, R. Müller, and E. E. B. Campbell, *Z. Phys. D* **40**, 361 (1997).
  - <sup>12</sup> L. A. Girifalco, *J. Phys. Chem.* **96**, 858 (1992).
  - <sup>13</sup> C. Rey, L. J. Gallego, and J. A. Alonso, *Phys. Rev. B* **49**, 8491 (1994).
  - <sup>14</sup> D. J. Wales, *J. Chem. Soc., Faraday Trans.* **90**, 1061 (1994).
  - <sup>15</sup> J. P. K. Doye and D. J. Wales, *Chem. Phys. Lett.* **262**, 167 (1996).
  - <sup>16</sup> T. P. Martin, T. Bergmann, H. Göhlich, and T. Lange, *Chem. Phys. Lett.* **172**, 209 (1990).
  - <sup>17</sup> J. P. K. Doye, D. J. Wales, and R. S. Berry, *J. Chem. Phys.* **103**, 4234 (1995).
  - <sup>18</sup> J. P. K. Doye and D. J. Wales, *Science* **271**, 484 (1996).
  - <sup>19</sup> J. P. K. Doye and D. J. Wales, *J. Phys. B* **29**, 4859 (1996).
  - <sup>20</sup> C. Rey, J. Garcia-Rodeja, and L. J. Gallego, *Z. Phys. D* **40**, 395 (1997).
  - <sup>21</sup> J. P. K. Doye, A. Dullweber, and D. J. Wales, *Chem. Phys. Lett.* **269**, 408 (1997).
  - <sup>22</sup> J. Garcia-Rodeja, C. Rey, and L. J. Gallego, *Phys. Rev. B* **56**, 6466 (1997).
  - <sup>23</sup> A. A. Shvartsburg and M. F. Jarrold, *Chem. Phys. Lett.* **86**, 261 (1996).
  - <sup>24</sup> W. Branz, N. Malinowski, H. Schaber, and T. P. Martin, *Chem. Phys. Lett.* **328**, 245 (2000).
  - <sup>25</sup> These temperatures are related to the time the clusters spend in the heating cell, which was approximately 0.5 ms.<sup>24</sup> If the heating time in the experiment is increased the temperatures for the observation of the icosahedral and non-icosahedral structures decrease somewhat. For example, for a heating time of 1 ms the decreases are 15-20 K.
  - <sup>26</sup> R. H. Leary and J. P. K. Doye, *Phys. Rev. E* **60**, R6320 (1999).
  - <sup>27</sup> J. P. K. Doye and D. J. Wales, *Phys. Rev. Lett.* **80**, 1357 (1998).
  - <sup>28</sup> C. L. Cleveland, W. D. Luedtke, and U. Landman, *Phys. Rev. Lett.* **81**, 2036 (1998).
  - <sup>29</sup> C. L. Cleveland, W. D. Luedtke, and U. Landman, *Phys. Rev. B* **60**, 5065 (1999).
  - <sup>30</sup> J. P. K. Doye, M. A. Miller, and D. J. Wales, *J. Chem. Phys.* **110**, 6896 (1999).
  - <sup>31</sup> J. P. Neirotti, F. Calvo, D. L. Freeman, and J. D. Doll, *J. Chem. Phys.* **112**, 10340 (2000).
  - <sup>32</sup> J. P. K. Doye and F. Calvo, *Phys. Rev. Lett.* **86**, 3570 (2001).
  - <sup>33</sup> F. Calvo, J. P. K. Doye, and D. J. Wales, *Phys. Rev. Lett.* submitted (2001).
  - <sup>34</sup> W. Zhang, L. Liu, J. Zhuang, and Y. Li, *Phys. Rev. B* **62**, 8276 (2000).
  - <sup>35</sup> F. Baletto, C. Mottet, and R. Ferrando, *Phys. Rev. B* **63**, 155408 (2001).
  - <sup>36</sup> J. P. K. Doye, M. A. Miller, and D. J. Wales, *J. Chem. Phys.* **111**, 8417 (1999).
  - <sup>37</sup> J. A. Northby, *J. Chem. Phys.* **87**, 6166 (1987).
  - <sup>38</sup> D. J. Wales, *J. Chem. Phys.* **101**, 3750 (1994).
  - <sup>39</sup> M. A. Miller, J. P. K. Doye, and D. J. Wales, *J. Chem. Phys.* **110**, 328 (1999).
  - <sup>40</sup> M. A. Miller, J. P. K. Doye, and D. J. Wales, *Phys. Rev. E* **60**, 3701 (1999).
  - <sup>41</sup> L. J. Gallego, J. Garcia-Rodeja, M. M. G. Alemany, and C. Rey, *Phys. Rev. Lett.* **83**, 5258 (1999).
  - <sup>42</sup> J. M. Pacheco and J. P. Prates-Ramalho, *Phys. Rev. Lett.* **79**, 3873 (1997).
  - <sup>43</sup> F. Calvo, *J. Phys. Chem. B* **105**, 2183 (2001).
  - <sup>44</sup> Y.-H. Luo, J. Zhao, S. Qiu, and G. Wang, *Phys. Rev. B* **59**, 14903 (1999).
  - <sup>45</sup> B. M. Axilrod and E. Teller, *J. Chem. Phys.* **11**, 299 (1943).
  - <sup>46</sup> D. J. Wales and J. Uppenbrink, *Phys. Rev. B* **50**, 12342 (1994).
  - <sup>47</sup> M. H. J. Hagen and D. Frenkel, *J. Chem. Phys.* **101**, 4093 (1994).
  - <sup>48</sup> J. P. K. Doye and D. J. Wales, *J. Chem. Soc., Faraday Trans.* **93**, 4233 (1997).

- <sup>49</sup> D. J. Wales, J. Chem. Soc., Faraday Trans. **86**, 3505 (1990).
- <sup>50</sup> J. Uppenbrink and D. J. Wales, J. Chem. Phys. **96**, 8520 (1992).
- <sup>51</sup> D. J. Wales and J. P. K. Doye, J. Phys. Chem. A **101**, 5111 (1997).
- <sup>52</sup> Z. Li and H. A. Scheraga, Proc. Natl. Acad. Sci. USA **84**, 6611 (1987).
- <sup>53</sup> D. J. Wales and H. A. Scheraga, Science **285**, 1368 (1999).
- <sup>54</sup> J. P. K. Doye, D. J. Wales, and M. A. Miller, J. Chem. Phys. **109**, 8143 (1998).
- <sup>55</sup> J. P. K. Doye, in *Global Optimization—Selected Case Studies*, edited by J. D. Pinter (Kluwer Academic, Dordrecht, 2001).
- <sup>56</sup> B. Hartke, Chem. Phys. Lett. **258**, 144 (1996).
- <sup>57</sup> J. P. K. Doye, Phys. Rev. E **62**, 8753 (2000).
- <sup>58</sup> C. J. Cerjan and W. H. Miller, J. Chem. Phys. **75**, 2800 (1981).
- <sup>59</sup> D. J. Wales *et al.*, Adv. Chem. Phys. **115**, 1 (2000).
- <sup>60</sup> D. J. Wales, J. P. K. Doye, A. Dullweber, M. P. Hodges, F. Y. Naumkin and F. Calvo, The Cambridge Cluster Database, URL <http://www-wales.ch.cam.ac.uk/CCD.html>.
- <sup>61</sup> F. Baletto, C. Mottet, and R. Ferrando, Phys. Rev. Lett. **84**, 5544 (2000).
- <sup>62</sup> F. H. Stillinger and D. K. Stillinger, J. Chem. Phys. **93**, 6013 (1990).
- <sup>63</sup> R. E. Kunz and R. S. Berry, Phys. Rev. Lett. **71**, 3987 (1993).
- <sup>64</sup> O. M. Becker and M. Karplus, J. Chem. Phys. **106**, 1495 (1997).
- <sup>65</sup> D. J. Wales, M. A. Miller, and T. R. Walsh, Nature **394**, 758 (1998).
- <sup>66</sup> P. E. Leopold, M. Montal, and J. N. Onuchic, Proc. Natl. Acad. Sci. USA **89**, 8271 (1992).
- <sup>67</sup> J. D. Bryngelson, J. N. Onuchic, N. D. Socci, and P. G. Wolynes, Proteins: Structure, Function and Genetics **21**, 167 (1995).
- <sup>68</sup> D. R. Nelson and F. Spaepen, Solid State Phys. **42**, 1 (1989).
- <sup>69</sup> D. J. Wales, Mol. Phys. **78**, 151 (1993).
- <sup>70</sup> J. P. K. Doye and D. J. Wales, J. Chem. Phys. **102**, 9659 (1995).
- <sup>71</sup> F. Calvo, J. P. K. Doye, and D. J. Wales, J. Chem. Phys. submitted (2001).
- <sup>72</sup> E. Marinari and G. Parisi, Europhys. Lett. **19**, 451 (1992).
- <sup>73</sup> R. H. Swendsen and J.-S. Wang, Phys. Rev. Lett. **57**, 2607 (1986).
- <sup>74</sup> F. Calvo and J. P. K. Doye, Phys. Rev. E **63**, 010902(R) (2001).
- <sup>75</sup> J. P. K. Doye and F. Calvo, J. Chem. Phys. to be submitted .
- <sup>76</sup> F. Baletto, J. P. K. Doye and R. Ferrando, unpublished.
- <sup>77</sup> A. Cheng and M. L. Klein, Phys. Rev. B **45**, 1889 (1992).
- <sup>78</sup> M. S. Deleuze and F. Zerbetto, J. Am. Chem. Soc. **121**, 5281 (1999).
- <sup>79</sup> Z. Gamba, Phys. Rev. B **57**, 1402 (1998).
- <sup>80</sup> J. P. Lu, X.-P. Li, and R. M. Martin, Phys. Rev. Lett. **68**, 1551 (1992).
- <sup>81</sup> M. Sprik, A. Cheng, and M. L. Klein, J. Phys. Chem. **96**, 2027 (1992).
- <sup>82</sup> T. Yildirim, A. B. Harris, S. C. Erwin, and M. R. Pederson, Phys. Rev. B **48**, 1888 (1993).

TABLE I: Energies and point groups for the putative global minima for  $(C_{60})_N$  clusters modelled by the PPR potential. The energies of these minima when reoptimized without the inclusion of the three-body term ( $E_2$ ) are also given. Structural assignments are given for all clusters with  $N \geq 13$ , where i stands for icosahedral, d for decahedral (d<sup>+</sup> have an overlayer on the {111} faces), f for fcc and c for close-packed (but not fcc). Fcc and close-packed structures can be unstrained.

$N$	PG	S	$E/eV$	$E_2/eV$	$N$	PG	S	$E/eV$	$E_2$	$N$	PG	S	$E/eV$	$E_2/eV$
3	$D_{3h}$		-0.793763	-0.800181	38	$O_h$	f	-38.726684	-40.164289	73	$C_s$	d	-82.892601	-86.232181
4	$T_d$		-1.574722	-1.600362	39	$C_{4v}$	f	-39.803068	-41.276819	74	$C_{5v}$	d	-84.275939	-87.683469
5	$D_{3h}$		-2.360685	-2.406624	40	$C_{2v}$	f	-40.879585	-42.389454	75	$D_{5h}$	d	-85.854200	-89.335316
6	$O_h$		-3.179823	-3.251103	41	$C_{2v}$	d	-42.050754	-43.620062	76	$C_s$	d	-86.943730	-90.469387
7	$D_{5h}$		-4.174831	-4.277606	42	$C_s$	d	-43.134640	-44.743772	77	$C_{2v}$	d	-88.287170	-91.870873
8	$C_s$		-4.971222	-5.095539	43	$C_{2v}$	d	-44.465028	-46.115661	78	$C_1$	d	-89.376306	-93.004550
9	$C_{2v}$		-5.979744	-6.139683	44	$C_s$	d	-45.548888	-47.250124	79	$D_{3h}$	c	-90.750950	-94.414956
10	$C_{3v}$		-6.941044	-7.136890	45	$C_{2v}$	d	-46.879111	-48.632640	80	$C_s$	c	-91.847206	-95.555790
11	$C_{2v}$		-7.890403	-8.122285	46	$C_s$	c	-47.964493	-49.771293	81	$C_{2v}$	c	-93.195399	-96.961852
12	$C_{5v}$		-8.910974	-9.191726	47	$C_{2v}$	d	-49.293304	-51.138897	82	$C_{2v}$	d	-94.475899	-98.305791
13	$I_h$	i	-10.203987	-10.556666	48	$C_{2v}$	d <sup>+</sup>	-50.835900	-52.786358	83	$C_{2v}$	c	-95.639897	-99.508789
14	$C_{3v}$	i	-11.010918	-11.384715	49	$C_s$	d <sup>+</sup>	-51.926724	-53.919060	84	$C_{2v}$	d	-96.907100	-100.839577
15	$C_{2v}$	i	-12.028948	-12.436957	50	$D_{3h}$	c	-53.354529	-55.400213	85	$C_{3v}$	c	-98.138499	-102.126340
16	$C_{2v}$	d	-13.017348	-13.429036	51	$C_s$	c	-54.449934	-56.540311	86	$C_{3v}$	c	-99.728365	-103.787568
17	$C_{2v}$	d	-14.088380	-14.538481	52	$C_{2v}$	c	-55.797330	-57.945711	87	$C_s$	c	-100.867536	-104.983413
18	$D_{5h}$	d	-15.163644	-15.653781	53	$C_s$	c	-56.892907	-59.085964	88	$C_s$	c	-102.173549	-106.335126
19	$C_{2v}$	d	-16.218799	-16.743185	54	$C_{2v}$	d	-58.306782	-60.570092	89	$C_s$	d <sup>+</sup>	-103.461268	-107.695215
20	$C_{2v}$	d	-17.274543	-17.832640	55	$C_{2v}$	d	-59.408665	-61.716335	90	$C_s$	d <sup>+</sup>	-104.807341	-109.095407
21	$C_s$	d <sup>+</sup>	-18.353074	-18.949300	56	$C_s$	d	-60.752438	-63.116143	91	$C_{3v}$	c	-106.302975	-110.678677
22	$C_1$	d <sup>+</sup>	-19.425310	-20.059762	57	$C_{2v}$	d	-62.098302	-64.517510	92	$C_s$	c	-107.397152	-111.806846
23	$C_s$	d <sup>+</sup>	-20.686563	-21.386861	58	$D_{3h}$	d <sup>+</sup>	-63.386632	-65.901565	93	$C_s$	c	-108.747951	-113.216329
24	$C_1$	d <sup>+</sup>	-21.759634	-22.497858	59	$T_d$	c	-64.769800	-67.323349	94	$C_s$	c	-110.100130	-114.626428
25	$C_{3v}$	d <sup>+</sup>	-22.957151	-23.760958	60	$C_s$	d	-65.887129	-68.480038	95	$C_{2v}$	d	-111.653413	-116.285755
26	$C_{2v}$	d <sup>+</sup>	-24.141029	-24.968567	61	$C_{3v}$	f	-67.169082	-69.798058	96	$C_s$	d	-112.771588	-117.460346
27	$C_s$	d <sup>+</sup>	-25.218788	-26.085977	62	$C_1$	d	-68.330220	-71.021579	97	$C_1$	d	-114.123353	-118.862596
28	$C_s$	d <sup>+</sup>	-26.403185	-27.334120	63	$C_s$	d	-69.702863	-72.458970	98	$C_s$	c	-115.518307	-120.295415
29	$D_{5h}$	d	-27.542310	-28.503488	64	$C_{2v}$	d	-71.278073	-74.107991	99	$C_s$	d	-117.079750	-121.959509
30	$C_{2v}$	d <sup>+</sup>	-28.649061	-29.682832	65	$C_{2v}$	d	-72.382930	-75.268852	100	$T_d$	c	-118.491490	-123.409546
31	$C_{2v}$	d	-29.963558	-31.028821	66	$C_s$	d	-73.720048	-76.664850	101	$D_{5h}$	d	-120.052347	-125.073354
32	$C_1$	d	-31.047706	-32.157893	67	$C_{2v}$	d	-75.059516	-78.062777	102	$C_{2v}$	d	-121.170243	-126.247600
33	$C_{2v}$	d	-32.386698	-33.555532	68	$C_1$	d	-76.157881	-79.200432	103	$C_s$	d	-122.516174	-127.652314
34	$C_1$	d	-33.469737	-34.683456	69	$C_1$	d	-77.504125	-80.605732	104	$C_{2v}$	d	-123.864106	-129.058381
35	$C_{2v}$	d	-34.807885	-36.080228	70	$C_s$	d	-78.872607	-82.039199	105	$C_s$	d	-124.981491	-130.232109
36	$C_1$	d	-35.889548	-37.206754	71	$C_{2v}$	d	-80.450302	-83.690481					
37	$C_{2v}$	d	-37.226573	-38.602386	72	$C_1$	d	-81.545223	-84.828030					